Materials & Design 209 (2021) 110012

Contents lists available at ScienceDirect

Materials & Design

journal homepage: www.elsevier.com/locate/matdes

Evaluation of the therapeutic potential of resveratrol-loaded nanostructured lipid carriers on autosomal recessive spastic ataxia of Charlevoix-Saguenay patient-derived fibroblasts

Özlem Şen [a,*], Melis Emanet [a,b], Attilio Marino [a], Melike Belenli Gümüş [a,c], Martina Bartolucci [d], Stefano Doccini [e], Federico Catalano [f], Giada Graziana Genchi [a], Filippo Maria Santorelli [e], Andrea Petretto [d], Gianni Ciofani [a,*]

[a] Istituto Italiano di Tecnologia, Smart Bio-Interfaces, Viale Rinaldo Piaggio 34, 56025 Pontedera, Pisa, Italy
[b] Sabanci University, Sabanci University Nanotechnology Research and Application Center (SUNUM), Universite Caddesi 27-1, 34956 Tuzla, Istanbul, Turkey
[c] Scuola Superiore Sant'Anna, The Biorobotics Institute, Viale Rinaldo Piaggio 34, 56025 Pontedera, Pisa, Italy
[d] IRCCS Istituto Giannina Gaslini, Via Gerolamo Gaslini 5, 16147 Genova, Italy
[e] IRCCS Fondazione Stella Maris, Molecular Medicine for Neurodegenerative and Neuro-Muscular Diseases Unit, Via dei Giacinti 3, 56128 Calambrone, Pisa, Italy
[f] Istituto Italiano di Tecnologia, Electron Microscopy Facility, Via Morego 30, 16163 Genova, Italy

HIGHLIGHTS

- Resveratrol-loaded NLCs have been proposed as therapeutic agents in ARSACS.
- Results demonstrated their antioxidant and anti-inflammatory abilities.
- Transcriptomics and proteomics confirm their therapeutic potentialities.

GRAPHICAL ABSTRACT

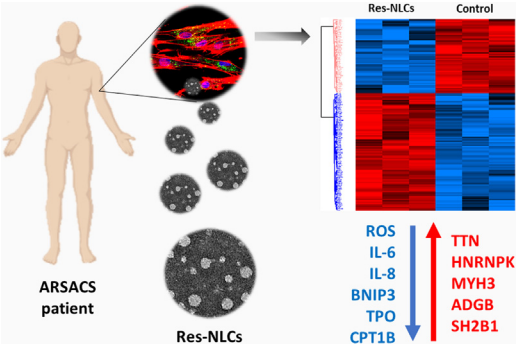

ARTICLE INFO

Article history:
Received 6 May 2021
Revised 23 July 2021
Accepted 26 July 2021
Available online 27 July 2021

Keywords:
Resveratrol
ARSACS
Nanostructured lipid carriers
Oxidative stress

ABSTRACT

Autosomal recessive spastic ataxia of Charlevoix-Saguenay (ARSACS) is a neurological disease characterized by autosomal recessive mutations in the sacsin gene (*SACS*), that cause in patients progressive cerebellar atrophy, damage of the peripheral nerves, and cognitive impairment. No effective therapies have been proposed for ARSACS, even if some evidences suggest that powerful antioxidant agents can be considered as a therapeutic tool. Resveratrol (Res) is a natural polyphenol compound derived from vegetal sources, the application of which in biomedicine is increasing in the latest years owing to its significant therapeutic effects, in particular in neurodegenerative diseases. In this study, we provide evidences about its potential exploitation in the treatment of ARSACS. Because of the low solubility of Res in physiological media, a nanoplatform based on nanostructured lipid carriers is proposed for its encapsulation and delivery. Resveratrol-loaded nanostructured lipid carriers (Res-NLCs) have been synthetized, characterized, and tested on healthy and ARSACS patient fibroblasts. Nanovectors displayed optimal stability and biocompatibility, and excellent antioxidant and anti-inflammatory activities. A comprehensive investigation

* Corresponding authors.
E-mail addresses: ozlem.sen@iit.it (Ö. Şen), gianni.ciofani@iit.it (G. Ciofani).

https://doi.org/10.1016/j.matdes.2021.110012

at gene (with real-time quantitative RT-PCR) and protein (with proteomics) level demonstrated the therapeutic potential of Res-NLCs, encouraging future investigations on pre-clinical models.

1. Introduction

Autosomal recessive spastic ataxia of Charlevoix-Saguenay (ARSACS) is a rare early-onset detrimental neurological disorder, caused by homozygote mutations in recessive *SACS* gene that encodes the sacsin protein. Sacsin localizes in mitochondria, and is crucial in neurons for physiological mitochondrial organization, morphology, and function [1,2]. Being mitochondrial dysfunction often correlated to excessive reactive oxygen species (ROS) production [3], many therapeutic approaches envisage the exploitation of antioxidants. In this direction, a previous work of our group tested idebenone, a synthetic analog of coenzyme Q_{10}, on ARSACS patient fibroblasts. Another example involves the use of docosahexaenoic acid (DHA), a phospholipid essential for central nervous system (CNS) development and responsible for the maintenance of neuronal physiological activities. This compound has been suggested as a therapeutic agent to improve brain functions in ARSACS disease by triggering anti-apoptotic and anti-inflammatory responses [4]. Baclofen is instead a synaptic reflex blocking agent that has been exploited as a therapeutic agent to reduce the symptoms in ARSACS patients, in terms of spasticity and muscle contractions [5]. Besides traditional pharmaceutical strategies, physical activity based on rehabilitation approaches has been also proposed to provide a symptomatic treatment in ARSACS patients [6].

The complexity of the CNS and the presence of the blood–brain barrier (BBB) however hinder the effectiveness of many compounds, that have to be loaded in nanotechnological platforms to promote their targeting and therapeutic efficiency [7]. Among the several options that nanomedicine offers, lipid-based nanosystems are particularly suitable for the delivery and targeting of hydrophobic compounds, given the protection and the stabilization that offer in physiological media [8]. Liposomes, solid lipid nanoparticles (SLNs), and nanostructured lipid carriers (NLCs) have been developed as drug delivery systems for an efficient drug accumulation at the level of the CNS [9], by providing drug stability, prolonged half-life, and tailored release of the therapeutic molecules [10]. NLCs, in particular, have been developed during the last decade as alternative and advantageous nanovectors with respect to more traditional SLNs. Composed by both solid and liquid lipids at physiological temperatures, NLCs provide high level of drug loading, excellent biocompatibility, tailorable biodegradation profiles, and are void of drug expulsion phenomena, instead typical of SLNs because of the crystallization of their inner solid core [11]. NLCs have been proposed for the delivery of curcuminoids [12], of itraconazole (an antifungal agent) [13], and of chemotherapy drugs [14,15].

In the present work, we exploit NLCs for the delivery and targeting of resveratrol (Res), as antioxidant agent in the treatment of ARSACS. Resveratrol, a powerful antioxidant of vegetal origin, was historically exploited in Asian traditional medicine against cardiovascular diseases [16]. Nowadays, the pharmaceutical potential of Res is confirmed by various studies that demonstrated its antioxidant, anti-inflammatory, anti-cancer, estrogenic, neuroprotective, cardioprotective, and anti-aging properties [17]. Promisingly, the antioxidant activity of Res has been assessed on Cr(VI)-dependent ROS overexpressing cells, and significant intracellular ROS reduction was observed jointly to a down-regulation of the inflammation stimulating factor NF-κB [18]. In another study, Res effects have been evaluated *in vivo* on a model of Alzheimer's disease, showing as the treatment reduced the amyloid plaque development in medial cortex, striatum, and hypothalamus [19]. Specifically, its anti-amyloidogenic activity was suggested to be triggered by the intracellular AMP-activated protein kinase (AMPK) activation, which leads to the decrement of extracellular Aβ accumulation [20].

Res is a sensitive compound, that is easily altered by chemical and physical stimuli such as light, oxidation, and hydrolysis; this makes difficult a direct administration of this antioxidant agent, and thus drug delivery nanoplatforms have been widely proposed in the literature. Res-loaded SLNs and NLCs have been developed to enhance the chemical stability of the compound and to improve skin absorption in a dermal delivery approach [21]. In another work, SLN encapsulation of Res enhanced its stability in blood circulation against rapid metabolization in liver and intestinal epithelial cells [22]. Moreover, the anti-transferrin receptor antibody (OX26) decoration of Res-SLNs promoted significant transcytosis across the BBB and distribution in CNS in *in vivo* models of Alzheimer's disease [22].

In the present study, we used resveratrol-loaded nanostructured lipid carriers (Res-NLCs) to decrease the oxidative stress in ARSACS patient cells owing to the Res excellent antioxidant properties. After extensive physicochemical characterization of the prepared nanovectors, the optimal dose in terms of biocompatibility and up-take rate was determined on both healthy and ARSACS patient fibroblasts. The effects on ROS production in *tert*-butylhydroperoxide (TBH)-stimulated healthy and ARSACS patient cells and on inflammatory cytokine release in lipopolysaccharide (LPS)-stimulated cultures were thoroughly analyzed. Extensive gene and protein expression analyses corroborated and confirmed collected results.

2. Results

2.1. Physicochemical characterization

NLCs have been prepared using glyceryl dibehenate as solid lipid, oleic acid as liquid lipid, poloxamer 188 as surfactant, and 1, 2-distearoyl-*sn*-glycero-3-phosphoethanolamine-poly(ethylene glycol) (DSPE-PEG) as colloidal stabilizer. Different formulations have been tested, as reported in Table S1, and being their characterizations showed in Table S2. All prepared formulations show good colloidal stability in water, with ζ-potential values below −29.0 mV. However, according to their production yields, four different NLC formulations have been selected for Res loading (namely NLCs_2, NLCs_5, NLCs_6, and NLCs_8), and their characterization is shown in Table S3. The hydrodynamic average size of NLCs_2, NLCs_5, NLCs_6, and NLCs_8 was found to be 154.0 ± 0.7 nm, 130.2 ± 1.2 nm, 104.4 ± 0.4 nm, and 92.4 ± 1.5 nm, respectively. After the Res loading, release from Res-NLCs has been preliminary assessed (data not shown), and according to this, the Res-NLCs_6 formulation (simply indicated in the following as Res-NLCs) was selected for further studies, because of the well-sustained Res release profile.

Fig. 1A depicts the structure of Res-NLCs; the characterization of NLCs and Res-NLCs has been performed by transmission electron microscopy (TEM) imaging as shown in Fig. 1B and 1C, respectively. Results indicate the presence of spherical and highly uniform NLCs and Res-NLCs. The hydrodynamic size distribution

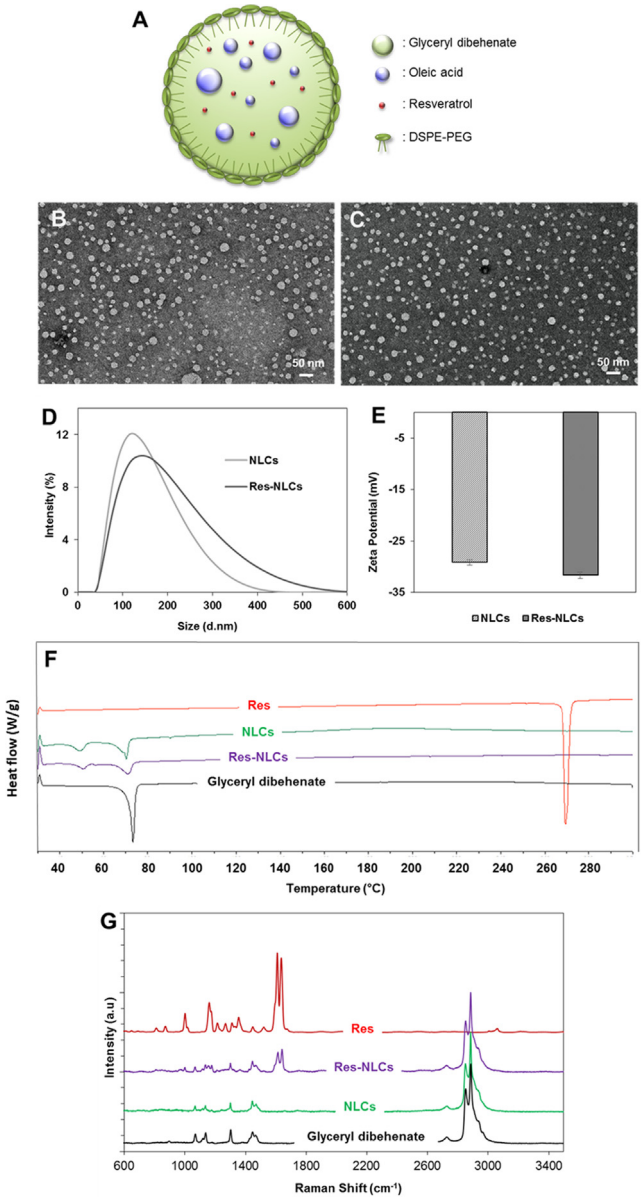

Fig. 1. A) Schematic representation of Res-NLCs. Representative TEM images of **B)** NLCs and **C)** Res-NLCs. **D)** Size distributions and **E)** ζ-potential measurements of NLCs and Res-NLCs. **F)** DSC thermograms and **G)** Raman spectra of Res, NLCs, Res-NLCs and glyceryl dibehenate.

assessed through dynamic light scattering (DLS) resulted 122.4 ± 1.2 nm and 142.0 ± 0.8 nm, respectively (Fig. 1D), while ζ-potential −29.2 ± 0.5 mV and −31.7 ± 0.6 mV (Fig. 1E). Long-term stability of NLCs and Res-NLCs has been monitored using DLS and ζ-potential measurements at 4 °C and at room temperature up to 60 days (Fig. S1): results showed that both NLCs and Res-NLCs remained stable at 4 °C. The particle size distributions showed good homogeneity, with polydispersity index (PDI) values < 0.3 [23]. At room temperature, however, a mild instability was found, suggesting 4 °C as long-term storing condition for our formulations. Differential scanning calorimetry (DSC) analyses have been performed to elucidate the physical state of the lipids used in NLCs and to correlate alterations with Res incorporation, as shown in Fig. 1F. The endothermic peak corresponding to the melting point of glyceryl dibehenate was found at 72.92 °C, while Res-NLC and NLC endothermic peaks were consistently detected at 70.83 °C and 70.16 °C, respectively. Besides, the endothermic peak of the free Res was found at 268.21 °C; the absence of this peak in the Res-NLCs suggests the absence of Res in crystalline state, confirming its loading in the amorphous lipid component [24]. Raman spectroscopy characterization was finally carried out (Fig. 1G). Free Res and Res-NLCs show similar peaks at around 1000 cm^{-1}, 1156 cm^{-1}, 1612 cm^{-1}, and 1638 cm^{-1} [25], while glyceryl dibehenate, NLCs and Res-NLCs samples have similar peaks at around 2850 cm^{-1} and 2884 cm^{-1} [26]. These further confirmed the successful entrapment of Res in NLCs; furthermore, the characteristic Res peak at around 1638 cm^{-1} was selected for label-free internalization analysis.

2.2. Drug loading, release, and antioxidant activity evaluation

The drug loading capacity (LC) and the encapsulation efficiency (EE) of Res-NLCs were assessed through both direct and indirect approaches (please check Experimental Section for details). In direct measurements, EE was found to be 90.3 ± 3.0%, while LC 2.35 ± 0.04% (Table S3); consistently, indirect measurements gave as result EE = 91.2 ± 3.0% and LC = 2.37 ± 0.03%. The percentage of encapsulated Res in NLCs was found to be satisfactorily high when compared to the literature [27]; finally, a production yield of 51.1 ± 3.8% was determined.

The cumulative Res released from Res-NLCs at different time points (1, 4, 24, and 72 h) and at different pH values (pH 9.0, 7.4, and 4.5) is reported in Fig. 2A. At the end-point of observation (72 h), 40.4 ± 2.1% of Res was released at pH 4.5, 31.6 ± 3.3% at pH 7.4, and 31.1 ± 1.2% at pH 9.0, denoting a slightly increased release extent at acidic pH value.

The antioxidant capacity of Res-NLCs was comparatively assessed with respect to the highest concentrations of free Res and bare NLCs by using a total antioxidant capacity assay

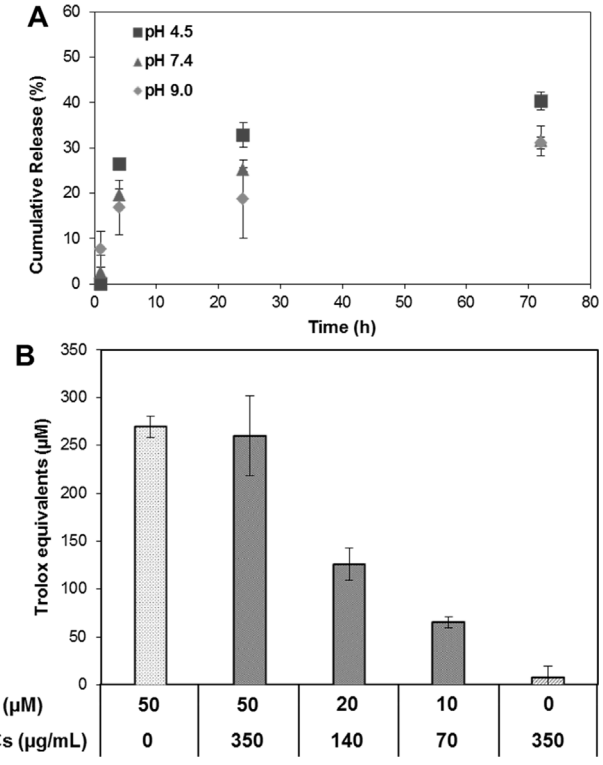

Fig. 2. A) Res release profile from Res-NLCs at several time points (1, 4, 24, and 72 h) and under different treatments (at pH 4.5, 7.4, and 9.0). **B)** Characterization of Res-NLCs antioxidant activity, expressed as Trolox equivalent. The values are presented as the mean ± standard error of 3 different measurements.

(Fig. 2B), and by exploiting Trolox, a water-soluble analogue of vitamin E, as reference. Results showed that 350 μg/mL of Res-NLCs (equivalent to 50 μM of free Res) have indeed comparable antioxidant capacity of 50 μM of Res, corresponding respectively to 269.0 ± 13.1 and 259.5 ± 41.7 μM of Trolox. Conversely, 140 μg/mL of Res-NLCs (corresponding to 20 μM of free Res) and 70 μg/mL of Res-NLCs (corresponding to 10 μM of free Res) show an equivalent of 126.0 ± 17.0 and 65 ± 5.7 μM of Trolox, respectively, suggesting a concentration-dependent Res-NLC antioxidant capacity.

2.3. Cytocompatibility investigation

The biocompatibility of Res-NLCs was evaluated *in vitro* on healthy and patient fibroblast cells by using Picogreen assay, an indirect indicator of cell proliferation that quantifies the total amount of DNA in a culture. Six different concentrations of Res-NLCs (14, 35, 70, 140, 350, and 700 μg/mL, corresponding to 2, 5, 10, 20, 50, and 100 μM of free Res) were tested in parallel with free Res and bare NLCs for 24 and 72 h. As shown in Fig. 3A and 3B, healthy and patient cells did not show any statistically significant decrease in cell viability after 24 h, while a significant increase (118 ± 2%) was observed on patient fibroblasts at the highest used Res-NLC concentration ($p < 0.05$). After 72 h of incubation, no statistically significant differences were found on healthy cells; a moderate increase (104 ± 1%) was again observed at the highest concentration of Res-NLCs. In ARSACS fibroblasts, no appreciable cytotoxic effects have been observed as well. Considering all these data, a precautionary concentration of 140 μg/mL Res-NLCs (corresponding to 20 μM of free Res) has been used in the following experiments.

2.4. Cellular internalization

Cellular localization of Res-NLCs in healthy and ARSACS fibroblasts has been qualitatively assessed after 24 h of incubation. Confocal microscopy imaging of fluorescently labeled Res-NLCs (green), F-actin (red), and nuclei (blue) are shown in Fig. 4A, denoting nanoparticles localized in the cytoplasm, and particularly in the perinuclear area; 3D confocal acquisitions are moreover showed in Fig. S2.

Confocal Raman microscopy was also exploited as complementary tool for label-free internalization assessment. Signal maps were originated basing on intensity of Res peak signature (Raman shift 1631 cm^{-1}–1664 cm^{-1}) and on that one of phenylalanine (indicating the cells, 980 cm^{-1}–1018 cm^{-1}) [28]. In Fig. 4B, these ranges can be seen on the representative spectra of patient and healthy fibroblasts incubated with Res-NLCs. The range and the related map that indicates the signal coming from Res-NLCs are depicted in green, while the range and the related map that indicates the signal coming from cells in red. Overall, extensive internalization in the perinuclear area is confirmed. Spectra and imaging of control cells (without Res-NLCs incubation) are reported for comparison in Fig. S3.

2.5. Oxidative stress

Intracellular oxidative stress levels of healthy (Fig. 5A and 5B) and ARSACS (Fig. 5C and 5D) fibroblasts were evaluated after two different experimental protocols (please check Experimental Section for details), designed to test ROS protective effects of Res-NLCs against intracellular ROS production (Treatment 1, Fig. 5A and 5C) or therapeutic effects of Res-NLCs in ROS-injured cells (Treatment 2, Fig. 5B and 5D). Intracellular ROS generation has been stimulated by TBH, and experiments have been carried out on both insulted (TBH^+) and non-insulted (TBH^-) cultures. In Treatment 1, fibroblasts have been simultaneously treated with Res-NLCs and TBH or just with Res-NLCs without TBH , in order to detect protective effects of Res-NLCs against oxidative stress. In Treatment 2, healthy and patient cells were first exposed to TBH to induce ROS production, and thereafter treated with Res-NLCs to evaluate therapeutic effects of Res-NLCs. ROS levels have been evaluated through flow cytometry following CellROX™ staining. Concerning healthy cells, we have in all cases a significant decre-

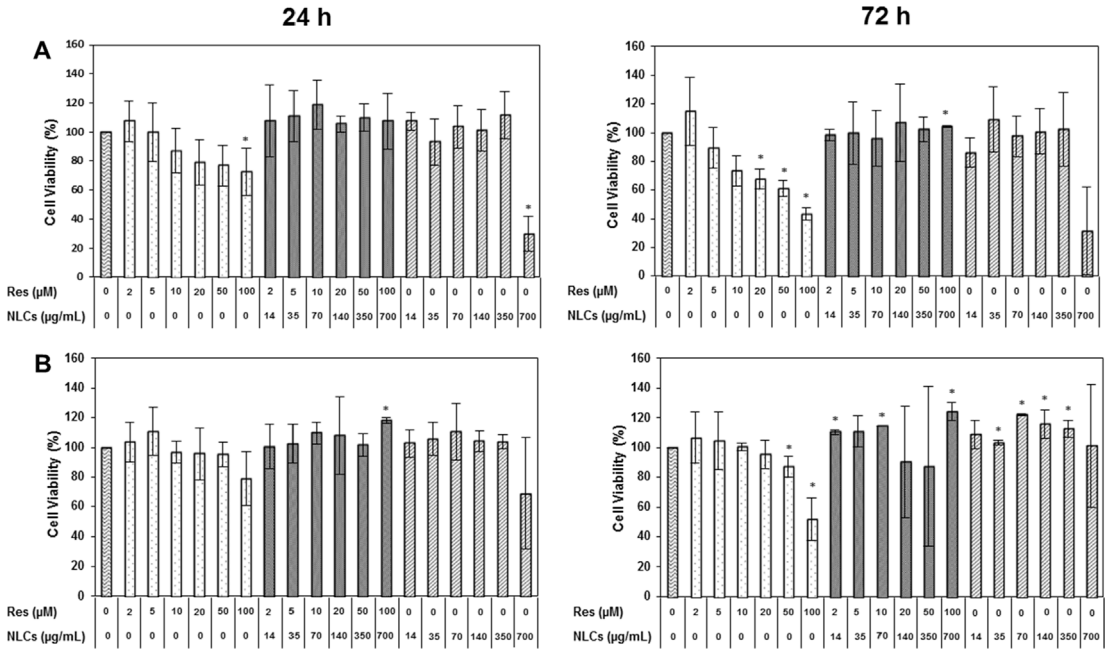

Fig. 3. Biocompatibility studies on **A)** healthy and **B)** ARSACS fibroblasts treated for 24 and 72 h with Res, Res-NLCs, and NLCs. The values are presented as the mean ± standard error of 3 different measurements (* $p < 0.05$).

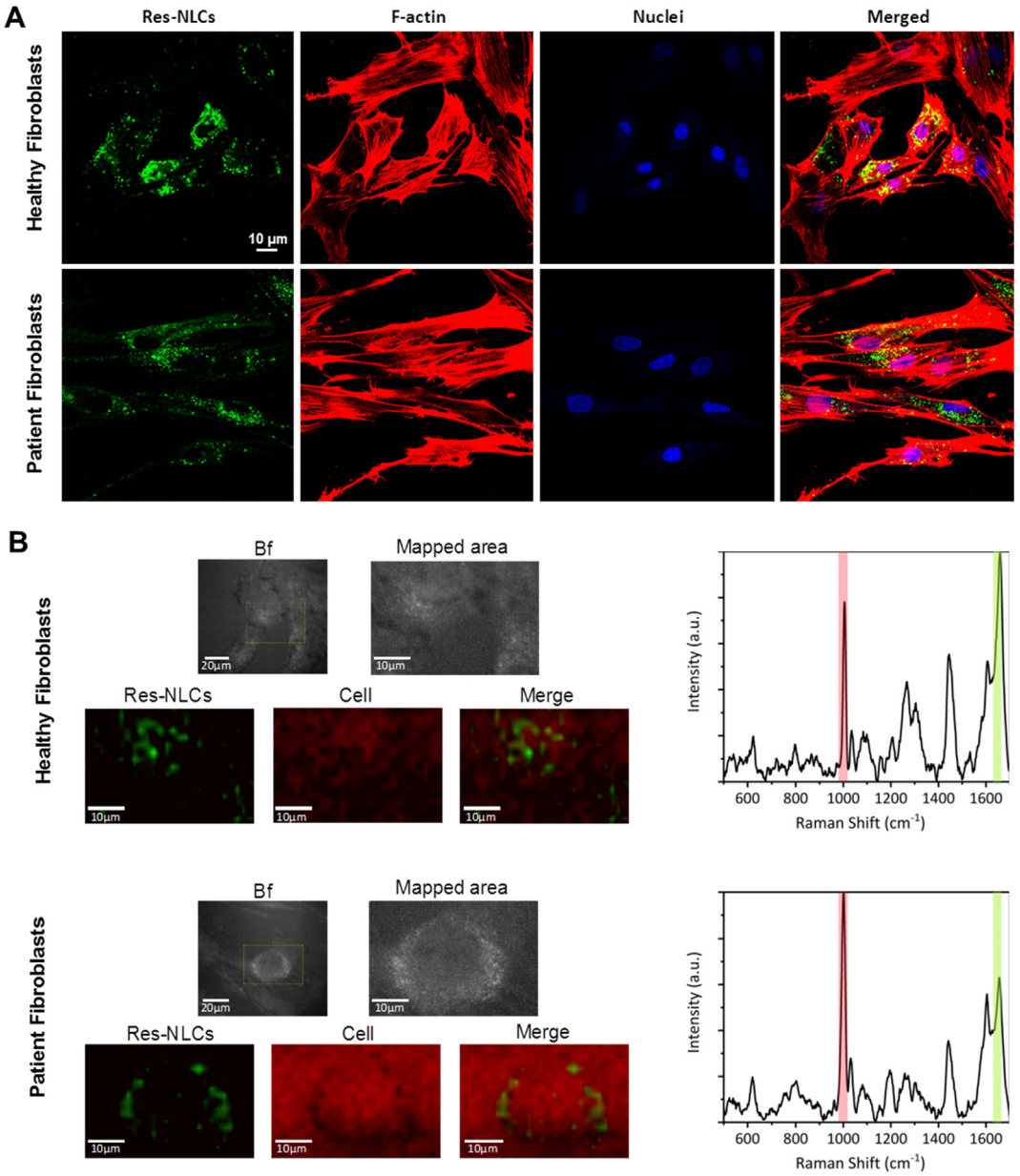

Fig. 4. A) Representative confocal images of healthy and patient fibroblasts treated for 24 h with fluorescently-labelled Res-NLCs (green). F-actin (red) and nuclei (blue) are also shown. **B)** Confocal Raman imaging of patient and healthy fibroblasts treated with Res-NLCs for 24 h. Representative Raman spectrum of the cells is also shown. Bright field (Bf) image and cropped Bf image of mapped area are shown for both samples, followed by Raman signal indicating Res-NLCs (Raman shift range: 1631 cm^{-1}-1664 cm^{-1}), Raman signal indicating cells (Raman shift range: 980 cm^{-1}-1018 cm^{-1}), and merged image of Raman signals originating from Res-NLCs and cells. Red and green colored areas on the spectrum are associated with the spectral range of cells and Res-NLCs, respectively. (For interpretation of the references to colour in this figure legend, the reader is referred to the web version of this article.)

ment of ROS-positive cells in the presence of Res-NLCs. A moderate, yet significant, effects was found also in Treatment 2 following incubation of TBH^+ cultures with plane Res and empty NLCs (most probably because of a mild antioxidant activity of the lipids). A similar trend was confirmed in ARSACS cultures, for both treatments, with the exception of Treatment 1 in non-stimulated cells, where conversely Res and Res-NLCs showed a mild increment of ROS-positive cells.

Representative flow cytometry scatter plots of experiments are reported in Figs. S4 and S5. Furthermore, morphological changes in healthy and patient fibroblasts after Treatment 1 and 2 were monitored using bright-field microscopy, and qualitative assessment of the culture status is in line with the quantitative ROS evaluation (Figs. S6–S9).

2.6. Cytokine production

The effects of different treatments on the inflammatory cytokines interleukin 6 (IL-6) and interleukin 8 (IL-8) have been evaluated on lipopolysaccharides (LPS)-stimulated healthy and patient fibroblasts (Fig. 6). First of all, the effects of bare Res on IL-6 and IL-8 release have been evaluated after both Treatment 1 and 2. As shown in Fig. 6A, following Treatment 1, release of IL-6 was not statistically different with respect to the control cultures; while a significant ($p < 0.05$) decrement of IL-8 release from 163.8 ± 10.8 pg/μg to 82.4 ± 4.6 pg/μg was found. Considering Treatment 2, a significant decrement in IL-6 (from 95.8 ± 4.8 pg/μg to 75.8 ± 2.3 pg/μg) and IL-8 levels (from 163.8 ± 10.8 pg/μg to 59.2 ± 4.1 pg/μg) has been found in healthy fibroblasts (Fig. 6B). As

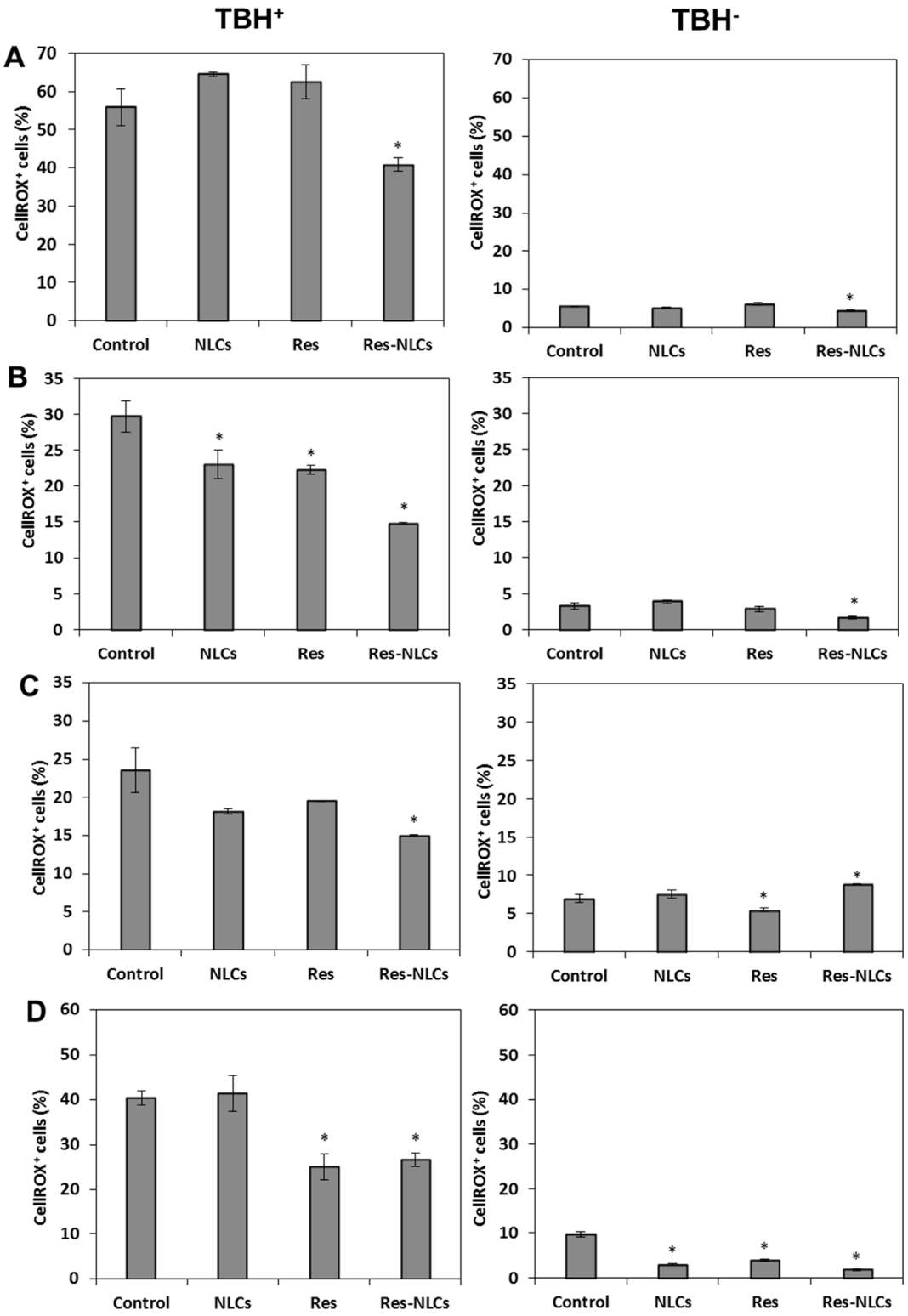

Fig. 5. Percentage of CellROX$^+$ cells in healthy fibroblast cultures after **A)** Treatment 1 and **B)** Treatment 2, with and without TBH insult. Percentage of CellROX$^+$ cells in ARSACS fibroblast cultures after **C)** Treatment 1 and **D)** Treatment 2, with and without TBH insult. The values are presented as the mean ± standard error of 3 different measurements (* $p < 0.05$).

shown in Fig. 6C, cytokine release decreased also in patient fibroblasts after Treatment 1; specifically, IL-6 release decreased from 300.7 ± 5.8 pg/μg to 237.1 ± 0.6 pg/μg and IL-8 release decreased from 360.2 ± 23.4 pg/μg to 246.9 ± 16.4 pg/μg. However, after Treatment 2, only IL-6 release from patient fibroblasts significantly decreased from 104.2 ± 4.7 pg/μg to 75.5 ± 0.2 pg/μg, as seen in Fig. 6D. When cultures were treated with Res-NLCs and LPS simultaneously (Treatment 1), IL-6 and IL-8 levels significantly ($p < 0.05$) decreased to 125.5 ± 6.3 pg/μg and 55.3 ± 0.5 pg/μg from 180.8 ± 1 3.9 pg/μg and 168.2 ± 4.2 pg/μg, respectively, in LPS-stimulated

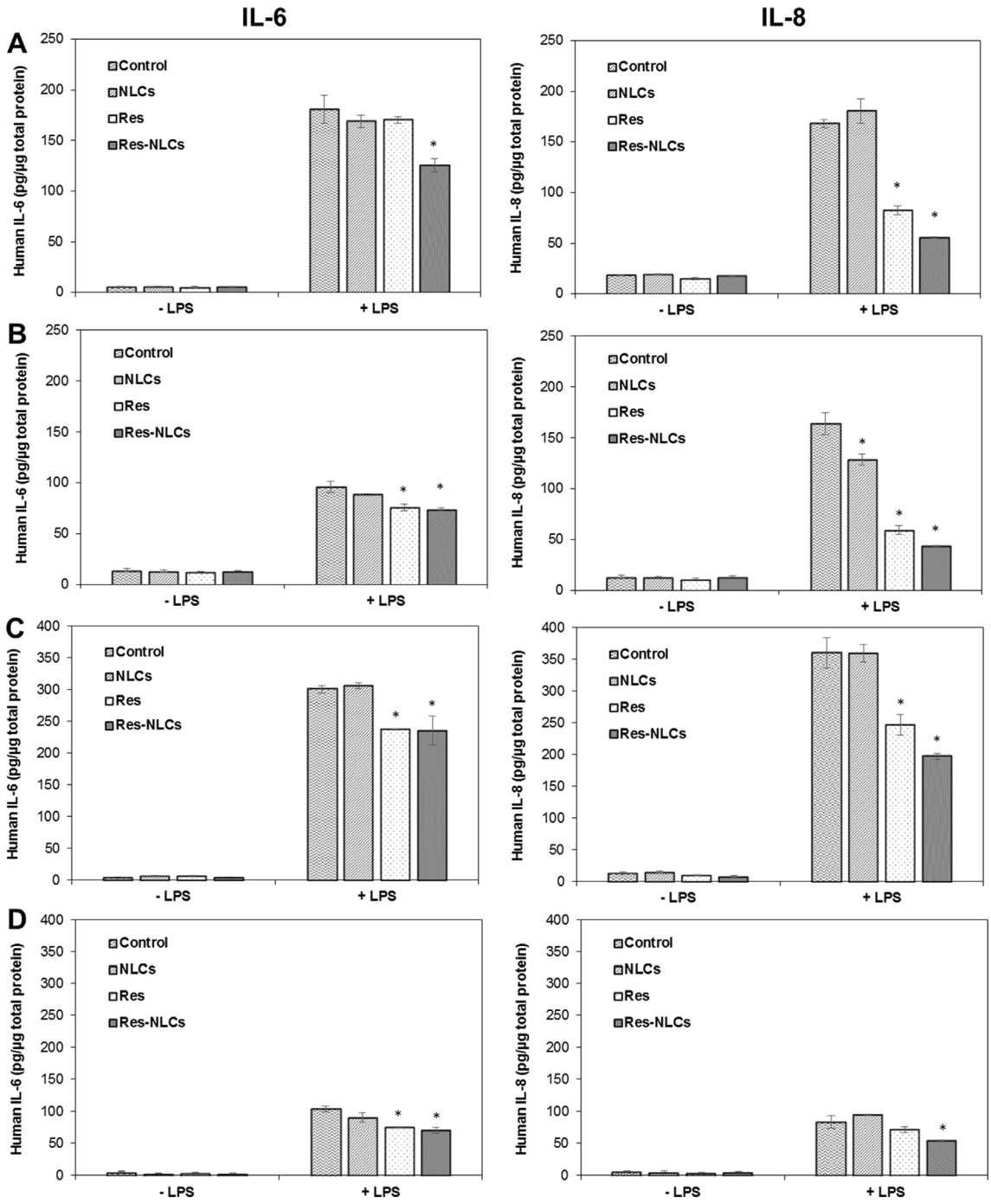

Fig. 6. Detection of IL-6 and IL-8 release from healthy fibroblasts after **A)** Treatment 1 and **B)** Treatment 2, and from ARSACS fibroblasts after **C)** Treatment 1 and **D)** Treatment 2. Results have been normalized over the total protein content (* $p < 0.05$).

cells treated with Res-NLCs with respect to LPS-stimulated control cultures (Fig. 6A). Fig. 6B shows the effect of Res-NLCs after a pre-incubation with LPS (referred as to Treatment 2). In this treatment, IL-6 levels significantly decreased to 73.8 ± 0.2 pg/µg from 95.8 ± 4.8 pg/µg on the cells treated with Res-NLCs, while the decrease of IL-8 levels was more pronounced (from 163.8 ± 10.8 pg/µg to 43.6 ± 0.2 pg/µg). Concerning patient fibroblasts, Fig. 6C shows a significant decrement of IL-6 levels (from 300.7 ± 5.8 pg/µg to 235.5 ± 22.5 pg/µg) and of IL-8 levels (from 360.2 ± 23.4 pg/µg to 197.2 ± 4.7 pg/µg) on cells treated with Res-NLCs after Treatment 1. As shown in Fig. 6D, Res-NLCs decreased the IL-6 and IL-8 levels significantly in patient fibroblasts as well after Treatment 2. IL-6 levels decreased from 104.2 ± 4.7 pg/µg to 70.5 ± 4.4 pg/µg, while IL-8 levels from 83.6 ± 9.5 pg/µg to 54.7 ± 0.7 pg/µg with respect to control cultures. No differences were observed among all the experimental groups of all the treatments in cultures without LPS stimulation, as well as in the treatment with plain NLCs.

2.7. Gene transcription and proteomics

Transcription profile of genes involved in oxidative stress and mitochondrial functionalities has been evaluated on ARSACS fibroblasts with and without Res-NLC treatments. Results are reported in Fig. 7 and in Tables S4 and S5. After Res-NLCs treat-

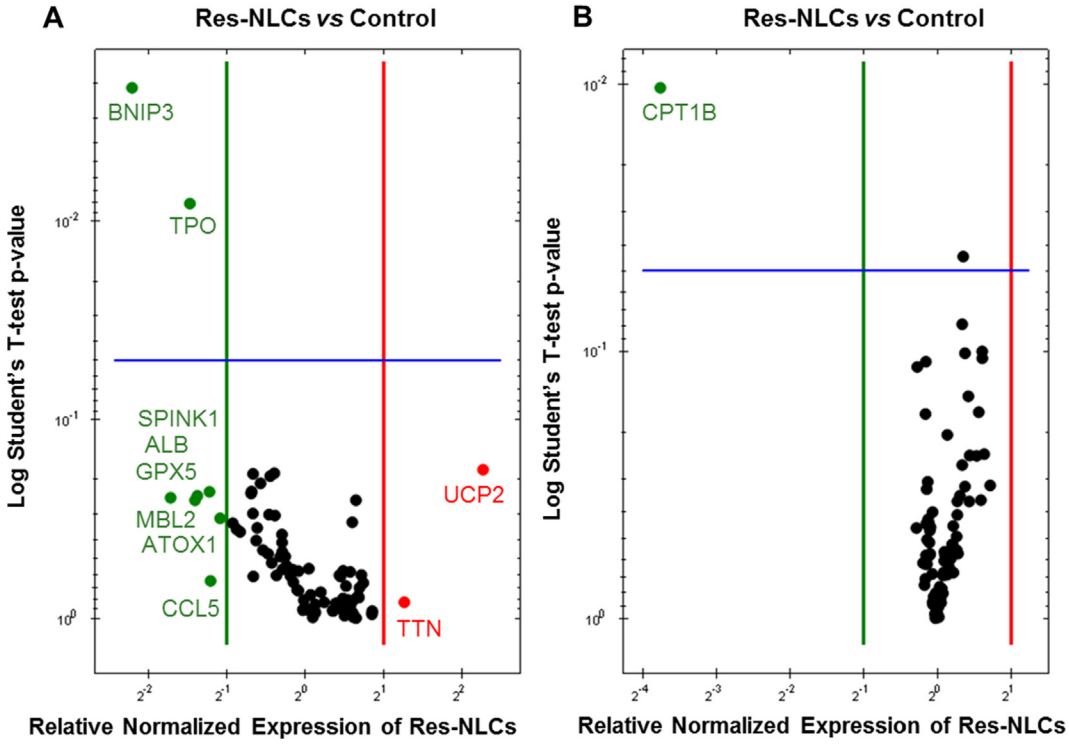

Fig. 7. Volcano plots showing up- and down-regulation of **A)** oxidative stress-related genes and **B)** mitochondria-related genes on patient fibroblasts treated with Res-NLCs (140 μg/mL) with respect to control cultures (0 μg/mL).

ment, we found statistically significant down-regulation of *BNIP3* (coding for BCL2 interacting protein 3) and of *TPO* (coding for thyroid peroxidase) among genes related to the oxidative stress. Despite statistically non-significant, an important down-regulation was also found for *SPINK1* (serine peptidase inhibitor Kazal type 1), *ALB* (albumin), *GPX5* (glutathione peroxidase 5), *MBL2* (mannose binding lectin 2), *ATOX1* (ATX1 antioxidant protein 1 homolog), and *CCL5* (chemokine (C-C motif) ligand 5); *UCP2* (uncoupling protein 2) and *TTN* (titin) were instead up-regulated (Fig. 7A). Among mitochondria-related gene, a statistically significant down-regulation of *CPT1B* (carnitine palmitoyltransferase) was observed upon Res-NLC treatment (Fig. 7B).

Proteomic analysis was analogously carried out on ARSACS fibroblasts either treated or not with Res-NLCs, and results are depicted in Fig. 8. A significant over-expression (6-fold, $p < 0.05$) was detected for titin, heterogeneous nuclear ribonucleoprotein K, androglobin, and myosin-3; while polyhomeotic-like protein 2 and E3 ubiquitin-protein ligase NRDP1 were 4-fold over-expressed (Fig. 8A). Significant under-expression (6-fold, $p < 0.05$) was instead found for rRNA/tRNA 2-O-methyltransferase fibrillarin-like protein 1 and Rho GTPase-activating protein 31, while 4-fold under-expression was found for ATP-dependent RNA helicase and methyl-CpG-binding domain protein 4. A heatmap reporting all the over-expressed (in red) and under-expressed (blue) analyzed proteins is depicted in Fig. 8B.

3. Discussion

In this study, ARSACS patient fibroblasts have been considered as an *in vitro* model of this pathology, since their phenotype allows correlation between metabolism and disease to be evaluated [29–31]. Pathological cells have been comparatively investigated along with normal healthy fibroblasts, for the assessment of antioxidant and anti-inflammatory effects of resveratrol-loaded nanovectors. In the recent years, resveratrol became particularly popular in biomedicine because of the so-called "French paradox", a phenomenon depicting the low incidence of cardiovascular diseases in French people despite their high-fat diet [32]. Resveratrol acts as a free radical scavenger because of the redox features of its phenolic hydroxyl groups; moreover, it owns the ability to trigger several intracellular antioxidant enzymes [33]. It is reported that high doses of resveratrol (up to 5 g daily) could improve the neurologic function in Friedreich's ataxia, which is an autosomal recessive neurodegenerative disorder [34].

Because of the insolubility of the resveratrol in aqueous media, in this study we adopted an encapsulation in nanostructured lipid carriers. NLCs have been preferred with respect to other nanocarrier typology since they usually present high drug loading, sustained drug release, and are void of drug expulsion phenomena due to the crystallization of the inner solid core (phenomenon instead typical in SLNs). Furthermore, some studies point out a better cell internalization extent of NLCs when compared to SLNs [21]. In our formulation, glyceryl dibehenate has been chosen as solid lipid, since it further promotes a high drug loading, allowing the long chain length of behenic acid the intermolecular entrapment of drug molecules [35]. Another important feature in the preparation of NLCs is the choice of the surfactants, that control the size and the stability of the particles, preventing their aggregation even in long-storage conditions. Poloxamer 188 was exploited due to its excellent ability to decrease surface tension while guaranteeing, at the same time, high biocompatibility [36]. Our results showed that obtained nanovectors presented optimal stability and size distribution (up to 2 months) suitable for cellular investigation [37], excellent biocompatibility, and dose-dependent antioxidant activity comparable to that one of bare Res.

Calorimetric analysis on Res-NLCs, Res, NLCs, and glyceryl dibehenate indicates the high stability of the lipids even following the Res encapsulation. Moreover, the typical DSC resveratrol peak was lost upon NLC encapsulation, suggesting its successful solubilization in the liquid lipid phase [21].

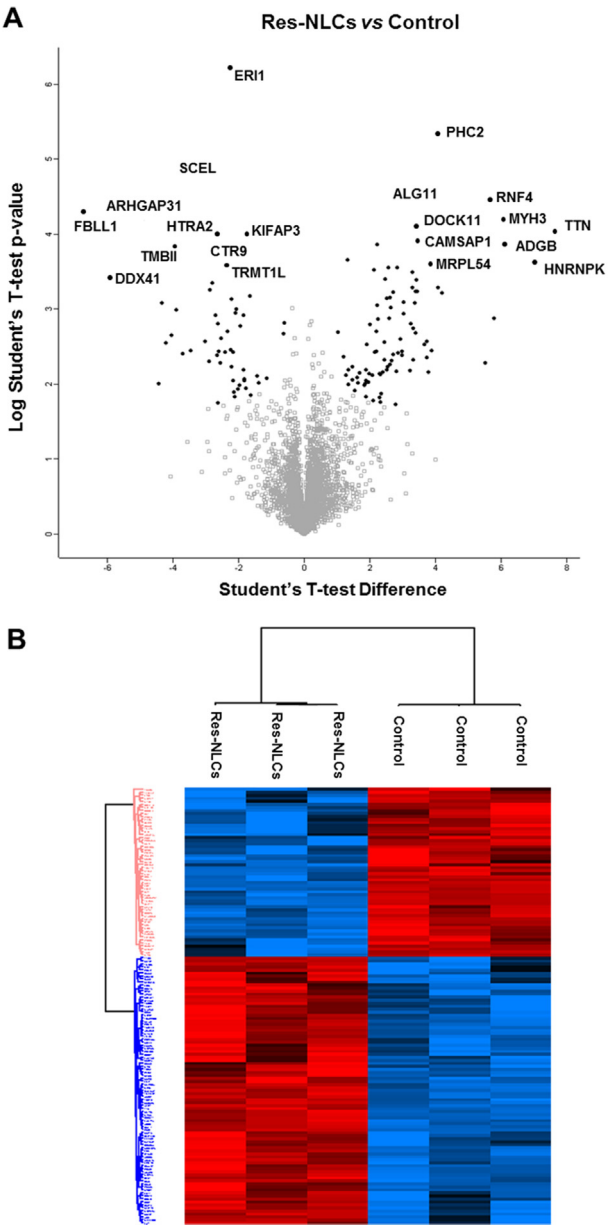

Fig. 8. A) Volcano plot and **B)** heatmap showing over- and under-expression of proteins in Res-NLCs-treated (140 μg/mL) ARSACS fibroblasts with respect to control cultures.

A major signature in ARSACS cells is the over-production of ROS, that correlates with a decreased mitochondrial function [3]. In particular, mutations occur in *SACS* gene encoding sacsin, a protein localized on the mitochondrial membrane, supposedly involved in the respiratory chain. In ARSACS cells, the mitochondrial functionality is highly impaired, and this is reflected into a decrement of the respiratory chain activity, that leads to lower ATP synthesis and ROS over-production [30]. Here, we showed as Res-NLCs limited oxidative stress, even in presence of a pro-oxidant stimulus; moreover, Res-NLCs resulted to be more efficient with respect to bare Res, most probably because of an improved stability of the antioxidant agent in aqueous environment [38].

Chronic neuroinflammation plays a key role in neurodegenerative disorders, and it leads to development of pathological conditions such as Alzheimer's disease, Parkinson's disease, multiple sclerosis, and glioblastoma [39]. Furthermore, chronic neuroinflammation is stimulated by a continuous secretion of inflammation stimulatory cytokines [40]. Therefore, in this study, release of inflammatory cytokines IL-6 and IL-8 has been evaluated upon LPS stimulation, and protective effects of Res-NLCs have been demonstrated. As many other cytokines, IL-6 and IL-8 are key factors in generation of inflammation in case of exposure to infections and toxins. [41]. However, despite their involvement in recovery actions, over-production of IL-6 and IL-8 can cause a chronic neuroinflammation [42]. In an interesting study, Res showed a promising efficiency against neuroinflammation by suppressing IL-1β, IL-6, and TNF-α secretion from glial cells [43]. Res treatment also up-regulated the expression of the suppressor of cytokine signalling-1 (*SOCS-1*), supporting the hypothesis of its role in neuroinflammation reduction. Moreover, resveratrol has been reported to decrease LPS-induced IL-8 production *via* regulating p38 MAPK, ERK1/2, and NF-κB activity [44]. In our study, Res-NLCs-treated healthy and patient cells showed statistically significant decrease in IL-6 and IL-8 levels, in agreement with the literature [45].

The alteration of regulation of several genes related to ROS metabolism was further evaluated using qRT-PCR, and we found statistically significant down-regulation of *BNIP3* and *TPO* genes. In the literature, there is considerable debate regarding *BNIP3*; some studies indicate that BNIP3 could induce cell death by competing with beclin-1 to bind to Bcl-2, and binding to Rheb thus blocking its activity and leading to autophagic cell death [46]; conversely, other evidences demonstrate that *BNIP3* could promote cell survival through a NF-κB mediated silencing [47]. Pan *et al.* found that *BNIP3* down-regulation in smooth muscle cell culture results in loss of mitochondrial matrix structure [48]. Our finding of a down-regulation of *BNIP3* upon Res-NLCs administration may be indicative of Res-NLC capability of modulating mitochondrial activity; however, further studies are required to assess the mechanism. *TPO* is mainly involved in autoimmune thyroid disorders [49], but neurological manifestations related to autoimmune thyroid disorders have been frequently indicated in the literature [50]. Correia *et al.*, as an example, revealed high anti-TPO antibody titers for a 61-year-old female patient, leading to a diagnosis of encephalopathy associated with autoimmune thyroid disease, characterized by neurological symptoms [51]. Despite no relevant alteration of the thyroid function has been found in ARSACS patient [52], it is however interesting to highlight *TPO* down-regulation on ARSACS fibroblasts upon Res-NLCs treatment, in line with other studies that show resveratrol-induced *TPO* down-regulation [53].

Among the 84 mitochondria-related genes we investigated, a significant down-regulation upon Res-NLC treatment was found for *CPT1B*. Localized on the outer mitochondrial membrane, the protein coded by this gene plays an important role in muscle mitochondrial β-oxidation of long-chain fatty acids [54]. In the literature, up-regulation of *CPT1B* is reported in post-traumatic stress disorder, which is associated with mitochondrial dysfunction in the brain [55]. Conversely, the inhibition of *CPT1B* is correlated with decreased ROS production, most probably because of the inhibition of fatty acid oxidation [56]. Altogether, *CPT1B* down-regulation can be an important marker highlighting rescue of ARSACS cells from ROS overproduction.

Proteomics analysis showed significantly modulated proteins associated to the Res-NLC treatment on ARSACS fibroblasts. Titin and heterogeneous nuclear ribonucleoprotein K were significantly over-expressed (6-fold). Titin plays a role during myogenesis, by providing elasticity to muscle and contributing to several signaling functions [57]. It is one of the 10 most frequently reported marker in neuromuscular disorders (2249 neurology patients), and it is a top contributor to congenital myopathy [58]; furthermore, variation in titin expression was identified by whole-exome sequencing in ARSACS patient [59]. Since the mutation in titin causes several different muscle disorders [60], the over-expression of titin upon administration of Res-NLCs encourages further investigations on the applicability of Res-NLCs as therapeutic agents in a wide range

of neuromuscular pathologies. Heterogenous nuclear ribonucleoproteins represent a large family of RNA-binding proteins, which contributes to several aspects of nucleic acid metabolism, including alternative splicing, transcriptional and translational regulation, and mRNA stabilization [61]. Given their extensive involvement in maintaining the functional integrity of the cell, it is not surprising that their dysfunction is involved in many neuropathological conditions, such as spinal muscular atrophy [62], amyotrophic lateral sclerosis [63], and multiple sclerosis [64]. In our study, we found a 6-fold over-expression of heterogeneous nuclear ribonucleoprotein K upon Res-NLC treatment, suggesting a positive effect in neurological diseases.

rRNA/tRNA 2-O-methyltransferase fibrillarin-like protein 1 and Rho GTPase-activating protein 31 were significantly under-expressed (6-fold) on ARSACS patient fibroblasts following Res-NLC treatment. Fibrillarin is involved in pre-ribosomal RNA processing, and catalyzes site-specific ribose methylation of ribosomal RNA [65]; it also interacts with the survival of motor neurons protein involved in spinal muscular atrophy, an autosomal neuromuscular recessive disease [66]. Our results, which indicate under-expression of rRNA/tRNA 2-O-methyltransferase fibrillarin-like protein 1, suggest an indirect protective role of Res-NLCs. The Rho GTPase-activating proteins are instead crucial in cell cytoskeletal organization, neuronal development, and synaptic functions [67]. Although RhoA activity is required for skeletal muscle cell differentiation [68], an *in vitro* study suggested that down-regulation of RhoA is essential for subsequent cell cycle withdrawal, expression of skeletal muscle differentiation genes, and myotube fusion [69]. Another study also demonstrated the down-regulation of Rho-GTPase-activating protein during skeletal muscle maturation and fusion [70]. Our finding of an under-expression of Rho GTPase-activating protein 31 on ARSACS patient cells upon Res-NLC administration may be an important finding for many pathological contexts; however, further investigations are still required.

Gene ontology (GO) analysis indicated significant over-expression of proteins involved in "protein containing complex subunit organization", "mRNA processing", "RNA splicing", "mRNA splicing, *via* spliceosome", "RNA splicing, *via* transesterification reactions with bulged adenosine as nucleophile", "RNA processing", "mRNA metabolic process", "protein-containing complex assembly", and "cellular component disassembly". The complete list of the significantly changed GO terms has been reported in Table S6. Autosomal recessive cerebellar ataxias have molecular pathogenesis including disorders of mitochondrial or cellular metabolism, and impairments of DNA repair or RNA processing functions [71]. The association between the defective mitochondrial mRNA maturation and spastic ataxia was demonstrated [72]; furthermore, it was suggested that mitochondrial dysfunction may result from abnormal mitochondrial RNA maturation and processing [73]. Morani *et al.* investigated the functional transcriptome analysis in ARSACS knockout neuronal-like SH-SY5Y cells [3], and found that the most differentially expressed genes are associated with RNA processing, which is in line with our findings. Finally, we would like to stress as proteomics-based strategies have been recently exploited in order to detect changes in protein levels of ARSACS patient cells, aiming at identifying biomarkers and functional pathways impaired in the disease, suggesting the importance of *-omics* technologies in elucidating the pathogenesis of ARSACS [74].

4. Conclusions

NLCs represent an excellent technology for drug delivery in neurological disease, presenting high drug loading, tunable drug release, excellent stability in long-term storage, and high biocompatibility. In addition, they can be produced at large-scale without using organic solvents, that are considered to decrease biocompatibility [75]. In this study, resveratrol-loaded NLCs have been successfully synthesized, and their antioxidant and anti-inflammatory effects demonstrated on an *in vitro* model of ARSACS. Our results show that the proposed nanovectors can be used as a protective and therapeutic agent to decrease oxidative stress and limit the production of inflammatory cytokines. Gene expression and proteomic analyses corroborated our findings, suggesting as Res-NLCs can play an important role against impaired mitochondrial function and supporting antioxidant defense mechanisms. Altogether, we can conclude as Res-NLCs can be considered a therapeutic tool in ARSACS, motivating future research towards *in vivo* pre-clinical studies. In particular, being ARSACS a neurological disease characterized by mitochondrial dysfunctions, targeting strategies to mitochondria might be the next step of this approach, to further improve the therapeutic efficacy of the proposed drug delivery system.

5. Experimental section

5.1. Preparation of NLCs

NLCs were fabricated using glyceryl dibehenate (Gattefossé SAS) as solid lipid, oleic acid (Sigma-Aldrich) as liquid lipid, poloxamer 188 (Sigma-Aldrich) as surfactant, and DSPE-PEG (Nanocs Inc.) as colloidal stabilizer. They were weighted according to Table S1 and mixed in MilliQ water. For resveratrol-loaded NLCs (Res-NLCs), resveratrol (Sigma-Aldrich) was weighted (0.01%, w/v) and added to the formulation with lipids. The lipids and the surfactant were heated at 75 °C, separately; thereafter, they were mixed and kept at 75 °C for 10 min. Next, the mixtures were sonicated using an ultrasonic tip (Fisherbrand™ Q125 Sonicator) for 10 min at 90% amplitude of power. At the end of the procedure, a step at 4 °C for at least 1 h followed. Obtained NLCs were filtered with a 0.2 μm filter (Sartorius Minisart Plus Syringe Filters) to eliminate aggregates; a further purification with an Amicon® Ultra-4 centrifugal filter (100 kDa, Sigma-Aldrich) at 7100*g* for 10 min was performed for three times. The samples were stored in plastic vials at 4 °C for further experiments.

For the preparation of fluorescently labeled Res-NLCs, 5 μM of Vybrant™ DiO dye (Invitrogen) was mixed with 1 mg/mL of Res-NLCs, and the mixture was stirred for 4 h at room temperature. A further purification step, to remove free dye, was performed as previously described with an Amicon® Ultra-4 centrifugal filter.

5.2. Dynamic light scattering and ζ-potential assessment

The colloidal stability of nanovectors was monitored in terms of size distribution and ζ-potential using a Zetasizer Nano NS (Malvern Instruments), upon dispersion in MilliQ water (10 μg/mL); the analyses have been performed at room temperature in triplicate. Long-term stability was assessed as well, storing samples at 4 °C and at room temperature for 2 months and periodically performing dynamic light scattering measurements.

5.3. Production yield (PY), entrapment efficiency (EE), loading capacity (LC), and release tests

Samples were frozen at −20 °C for 12 h, and then kept at −80 °C for 30 min. Thereafter, freeze-drying was carried out for 12 h using a FreeZone Freeze Dryer by Labconco. The production yield (PY) was calculated using the lyophilized sample according to Equation (1):

$$PY(\%) = \frac{(W_{theoretical} - W_{freeze-dried})}{W_{theoretical}} \times 100 \quad (1)$$

where $W_{theoretical}$ is the theoretical amount (in mg), and $W_{freeze\text{-}dried}$ is the freeze-dried amount (in mg) of the sample.

The EE and LC of Res-NLCs were directly measured after dissolving the lipids of the nanoparticles with a methanol:water (1:1 v/v) solution. Briefly, freeze-dried nanoparticles were dispersed in the methanol:water solution and kept at 75 °C for 2 h under stirring. Thereafter, samples were centrifuged at 7100*g* for 15 min. The supernatants were analyzed using a HPLC Shimadzu LC-20A for Res detection. The mobile phase was a mixture of methanol and water (52:48 v/v) with a flow rate of 1 mL/min. The injection volume and UV wavelength were set as 5 μL and 306 nm, respectively. Standard samples of Res in methanol:water mixture (1:1, v/v) have been previously prepared and analyzed in order to obtain a calibration curve (Fig. S10A).

The EE and LC of Res-NLCs were moreover indirectly measured by calculating the free Res present in the aqueous phase upon nanovector preparation using Eqs. (2) and (3), respectively. All the supernatants were collected after the washing steps and analyzed though HPLC as previously described.

$$EE(\%) = \frac{W_{total} - W_{free}}{W_{total}} \times 100 \quad (2)$$

$$LC(\%) = \frac{W_{total} - W_{free}}{W_{freeze-dried}} \times 100 \quad (3)$$

where W_{total} is the total amount of Res (in mg) used in the preparation, and W_{free} is the free Res present in the aqueous phase (in mg). $W_{freeze\text{-}dried}$ is the freeze-dried amount (in mg) of the sample.

Res cumulative release investigation has been performed in PBS at three different time points (1, 4, 24, and 72 h) and at different pH values (pH 4.5, 7.4, and 9.0), through HPLC analysis as previously described.

5.4. TEM imaging

Each sample (diluted 1:5 v/v) was adsorbed (for 20 s) on plasma-cleaned pure carbon 300 mesh copper grids. After several washing steps, the grids were negatively stained with a solution of uranyl acetate (1% in distilled water) for 60 s. The resulting samples were then analyzed in bright field mode using a JEOL JEM 1011 (JEOL) transmission electron microscope equipped with a thermionic source (W filament) operating at an acceleration voltage of 100 kV and with a Gatan Orius SC1000 series charge coupled device (CCD) camera (4008 2672 active pixels).

5.5. Differential scanning calorimetry (DSC) analysis

In order to assess nanovectors melting behavior, DSC analysis has been carried out on the lipid carriers as well as on the bulk materials (Res and glyceryl dibehenate), by using a differential scanning calorimeter DSC-1 STARe System (Mettler Toledo). Before the measurements, NLCs and Res-NLCs were freeze-dried, and the dried samples were weighted into the aluminum pans (0.5–1.0 mg). The measurements were performed under a nitrogen air atmosphere between 30 and 300 °C with a heat rate of 10 °C/min.

5.6. Raman spectroscopy analysis

Raman spectroscopy was performed on NLCs, Res-NLCs, Res, and glyceryl dibehenate using a Horiba LabRAM HR Evolution Raman microscope equipped with a 532 nm laser. All measurements were performed at least three times.

5.7. Total antioxidant capacity assay

Antioxidant features of Res-NLCs were measured using a total antioxidant capacity assay kit (Sigma-Aldrich) according to the manufacturer's instructions. Before starting, all reagents were allowed to reach to room temperature. Then, 100 μL of 70, 140, and 350 μg/mL Res-NLCs (corresponding to 10, 20, and 50 μM of resveratrol) were added into 96-well plates wells. 50 μM Res and 350 μg/mL of NLCs were used as positive and negative controls, respectively. For Trolox standards, 100 μL of 0, 80, 120, 160, 200, and 400 μM solutions were considered. 100 μL of Cu^{2+} working solution were thereafter added to all samples and standards. Following an incubation in the dark for 90 min, the absorbance was assessed at 570 nm using a Perkin Elmer Victor X3 microplate reader. A standard curve for the correlation of Trolox concentration to antioxidant capability was exploited (Fig. S10B).

5.8. Cell cultures

Human healthy fibroblasts (ATCC® PCS-201-012™) were cultured in Dulbecco's Modified Eagle's Medium (DMEM, Gibco) supplemented with 10% fetal bovine serum (FBS, Gibco), 1 mM sodium pyruvate (Gibco), 2 mM L-glutamine (Gibco), and 100 IU/mL of penicillin–streptomycin (Gibco). ARSACS patient fibroblasts derived from human skin punch biopsies were cultured in DMEM supplemented with 15% FBS, 10 ng/mL fibroblast growth factor (FGF, Sigma-Aldrich), 1 mM sodium pyruvate, 2 mM L-glutamine, 100 IU/mL of penicillin–streptomycin. Patient fibroblasts were collected according to standard procedures for diagnostic skin biopsies, and the study was carried out in accordance to the Declaration of Helsinki. Healthy and ARSACS patient fibroblasts at similar culture passages (P10–P15) were investigated.

5.9. Proliferation analysis: PicoGreen assay

For the proliferation analysis, healthy and ARSACS fibroblasts were seeded at $2{\cdot}10^4$ cells/cm^2 in 24-well plates, and analyzed using Quant-iT PicoGreen dsDNA assay kit (Invitrogen) following manufacturer's instruction. At 24 h from seeding, cells were treated with NLCs (14–700 μg/mL), Res-NLCs (14–700 μg/mL corresponding to 2–100 μM of Res) and Res (2–100 μM). After 24 and 72 h of incubation, cells were rinsed with PBS three times. Then, MilliQ water (500 μL) was added to the cells, and samples frozen at −80 °C. After three freezing and thawing cycles, the cells were analyzed with PicoGreen assay, which allows quantifying dsDNA content. Cell lysates (50 μL) were mixed with 100 μL of working solution, and then 150 μL of PicoGreen dye was added. Following incubation for 10 min in the dark, fluorescence was measured using a Perkin Elmer Victor X3 microplate reader (λ_{ex} = 485 nm; λ_{em} = 535 nm). The experiments were performed using two different cell batches and at least in triplicate.

5.10. Cellular internalization

For confocal microscopy imaging, cells were seeded at $2{\cdot}10^4$ cells/cm^2 in μ-Dishes (35 mm, Ibidi) and incubated for 24 h. Then, they were treated with 140 μg/mL DiO-labelled Res-NLCs for further 24 h. After incubation, the cells were fixed with 4% paraformaldehyde (PFA, Sigma-Aldrich) at 4 °C for 20 min and subsequently washed three times with PBS (Sigma-Aldrich). For the imaging of F-actin and nuclei, the cells were treated with TRITC-phalloidin (1:200, Sigma-Aldrich) and Hoechst (1:1000, Invitrogen) at 37 °C for 45 min. 2D images and 3D rendering were acquired with a confocal fluorescence microscope (C2 system Nikon).

Raman imaging was performed with a Horiba's LabRAM HR Evolution Confocal Raman Microscope equipped with 532 nm laser

in order to confirm uptake of Res-NLCs by patient-derived and healthy fibroblasts. Samples were prepared by seeding cells on Raman-grade calcium fluoride substrates (Crystran) at a seeding density of $2{\cdot}10^4$ cells/cm^2. After 24 h from seeding, cells were incubated with Res-NLCs at a concentration of 140 μg/mL for 24 h. Thereafter, cultures were fixed with 4% PFA in PBS for 20 min at 4 °C and analyzed immediately after fixation. Control groups without Res-NLCs treatment were prepared as well. Substrates with cells were kept in PBS during the analysis, and a 60 × immersion objective was used. Signal maps were constructed according to signal of Res-NLCs (Raman shift range: 1631 cm^{-1}–1664 cm^{-1}) and phenylalanine (Raman shift range: 980 cm^{-1}–1018 cm^{-1}), with a pixel intensity proportional to peak intensity (LabSpec 6 software). The green map of Res-NLCs and the red map of cells were merged by using ImageJ.

5.11. ROS detection

Healthy and ARSACS cells ($2{\cdot}10^4$ cells/cm^2) were seeded and incubated for 24 h at 37 °C. To investigate ROS protective effects of Res-NLCs in the presence of TBH (Sigma-Aldrich), the cells were treated with 200 μM TBH and Res (5 μM), NLCs (140 μg/mL), or Res-NLCs (140 μg/mL, corresponding to 5 μM of released Res) for 24 h (Treatment 1). To investigate the therapeutic capability of Res-NLCs on damaged cells, first the cells were treated with 200 μM TBH for 24 h; afterwards, cells were exposed to Res (5 μM), NLCs (140 μg/mL) or Res-NLCs (140 μg/mL, corresponding to 5 μM of released Res), and incubated for further 24 h (Treatment 2). After incubation, the cells were rinsed with PBS, detached from the plates using trypsin, and centrifuged at 1000*g* for 7 min at 4 °C. Thereafter, cells were stained with 5 μM CellROX™ Green Reagent (Invitrogen) for 15 min in PBS. The fluorescence intensity of the cells was measured using a Beckman Coulter CytoFLEX (λ_{ex} = 508-nm; λ_{em} = 525 nm).

5.12. Cytokine production

Lipopolysaccharides (LPS) was used to induce cytokine release from fibroblasts. Cells were seeded at $2{\cdot}10^4$ cells/cm^2, and 10 μg/mL of LPS was added to the cells with or without nanoparticles as described for ROS detection (Treatment 1 or Treatment 2, but using LPS instead of TBH). After incubation, the culture supernatants were collected and centrifuged at 1000*g* for 10 min in order to avoid any cellular debris. Human interleukin 6 (IL-6) and human interleukin 8 (IL-8) were analyzed using ELISA kits (ab178013 and ab46032, Abcam) according to the manufacturer's protocol. Data were normalized according to the total protein content of each sample. In order to perform protein extraction, the cultures were lysed using RIPA buffer (Sigma-Aldrich) and protease inhibitor (1:1000 v/v, Sigma-Aldrich). The protein content was measured using the bicinchoninic acid assay (BCA) kit (Sigma-Aldrich), following standard manufacturer's procedures.

5.13. Real-time quantitative RT-PCR

Transcription of oxidative stress- and mitochondria-related genes was investigated with real-time quantitative RT-PCR (qRT-PCR). Patient fibroblasts ($2{\cdot}10^4$ cells/cm^2) were seeded and incubated overnight for attachment. Thereafter, the cultures were treated with Res-NLCs (140 μg/mL) for 24 h; control cultures have been carried out as well. Total RNA was isolated using High Pure RNA Isolation kit (Qiagen) according to the manufacturer's protocol. RNA transcription into cDNA was carried out with 200 ng of RNA in a total volume of 20 μL, including 4 μL of iScript™ Reverse Transcription Supermix (5×, Bio-Rad). cDNA was analyzed with the Human Oxidative Stress RT^2 Profiler™ PCR Array (PAHS-065Y, Qiagen) and Human Mitochondria RT^2 Profiler™ PCR Array (PAHS-087Z, Qiagen), which profile the expression of 84 genes related to oxidative stress and mitochondria, respectively. In order to determine the transcription levels of genes, qRT-PCR was performed with SsoAdvanced™ Universal SYBR® Green Supermix (2×, Bio-rad) and using a CFX Connect™ Real-Time PCR Detection System (Bio-Rad). Finally, data were normalized by using multiple housekeeping genes including *ACTB*, *B2M*, *GAPDH*, *HPRT1* and *RPLP0*.

5.14. Proteomic analysis

For proteomic analysis, patient fibroblasts were seeded ($2{\cdot}10^4$ cells/cm^2) and left overnight to attach; thereafter, cultures have been either treated or not (as control) with 140 μg/mL of Res-NLCs for 24 h. Samples were lysed, reduced, and alkylated in 50 μL LYSE buffer (Preomics) at 95 °C for 10 min and sonicated with an Ultrasonic Processor UP200St (Hielscher), 3 cycles of 30 s. 50 μg of lysates samples were digested by adding trypsin and LysC at a 1:50 and 1:100 ratio of enzyme:protein content, respectively, and incubated at 37 °C overnight. Digested samples were processed by iST protocol [76].

Resulting peptides were analyzed by a nano-UHPLC-MS/MS system using an Ultimate 3000 RSLC coupled to an Orbitrap Fusion Tribrid mass spectrometer (Thermo Scientific Instrument). The mass spectrometry proteomics data have been deposited to the ProteomeXchange Consortium *via* the PRIDE [77] partner repository with the dataset identifier PXD025718. Elution was performed using a 200 cm uPAC C18 column (PharmaFluidics) mounted in the thermostated column compartment maintained at 50 °C. At first, it was applied a concentration gradient from 5% to 10% of buffer B (80% acetonitrile and 20% H_2O, 5% DMSO, 0.1% formic acid) coupled with a flow gradient from 750 nL/min to 350 nL/min for 15 min. Then, peptides were eluted with a 114 min linear gradient from 10% to 55% of buffer B at a constant flow rate of 350 nL/min. Orbitrap detection was used for MS1 measurements at a resolving power of 120,000 in a range between 375 and 1500 *m*/*z* and with a standard AGC target. Advanced peak detection was enabled for MS1 measurements. MS/MS spectra were acquired in the linear ion trap (rapid scan mode) after higher-energy C-trap dissociation (HCD) at a collision energy of 30% and with a Custom AGC target. For precursor selection, the least abundant signals in the three ranges 375–575 *m*/*z*, 574–775 *m*/*z*, and 774–1500 *m*/*z* were prioritized. Dynamic Exclusion was set at 25 s.

MaxQuant software [78], version 1.6.17.0, was used to process the raw data. The false discovery rate (FDR) for the identification of proteins, peptides, and PSM (peptide-spectrum match) was set to 0.01. A minimum length of 6 amino acids was required for peptide identification. Andromeda engine, incorporated into MaxQuant software, was used to search MS/MS spectra against Uniprot human database (release UP000005640_9606 December 2020). In the processing, the variable modifications were Acetyl (Protein N-Term), Oxidation (M) and Deamidation (NQ). Carbamidomethyl (C) was selected as fixed modification. Algorithm MaxLFQ was chosen for the protein quantification with the activated option "match between runs" to reduce the number of the missing proteins.

The intensity values were extracted and statistically evaluated using the ProteinGroup Table and Perseus software version 1.6.15.0 [79].

5.15. Statistical analysis

Data were analyzed using analysis of variance (ANOVA) followed by Bonferroni's *post-hoc* test in order to evaluate for signif-

icance, that was set at $p < 0.05$; data have been presented as mean value ± standard deviation of three independent experiments.

Declaration of Competing Interest

The authors declare that they have no known competing financial interests or personal relationships that could have appeared to influence the work reported in this paper.

Acknowledgements

This research was supported by the Italian Ministry of Health (grant no. RF-2016-02361610).

Data availability

The data required to reproduce these findings are available from the Corresponding Authors at reasonable request.

Appendix A. Supplementary material

Supplementary data to this article can be found online at https://doi.org/10.1016/j.matdes.2021.110012.

References

[1] A. Artero Castro, C. Machuca, F.J. Rodriguez Jimenez, P. Jendelova, S. Erceg, Short Review: Investigating ARSACS: models for understanding cerebellar degeneration, Neuropathol. Appl. Neurobiol. 45 (2019) 531–537, https://doi.org/10.1111/nan.12540.
[2] J.C. Engert, P. Berube, J. Mercier, C. Dore, P. Lepage, B. Ge, J.P. Bouchard, J. Mathieu, S.B. Melancon, M. Schalling, E.S. Lander, K. Morgan, T.J. Hudson, A. Richter, ARSACS, a spastic ataxia common in northeastern Quebec, is caused by mutations in a new gene encoding an 11.5-kb ORF, Nat. Genet. 24 (2000) 120–125, https://doi.org/10.1038/72769.
[3] F. Morani, S. Doccini, R. Sirica, M. Paterno, F. Pezzini, I. Ricca, A. Simonati, M. Delledonne, F.M. Santorelli, Functional Transcriptome Analysis in ARSACS KO Cell Model Reveals a Role of Sacsin in Autophagy, Sci. Rep. 9 (2019) 11878, https://doi.org/10.1038/s41598-019-48047-x.
[4] I. Ricca, A. Tessa, R. Trovato, G.M. Bacci, F.M. Santorelli, Docosahexaenoic acid in ARSACS: observations in two patients, BMC Neurol. 20 (2020) 1–4.
[5] V. Picher-Martel, N. Dupre, Current and promising therapies in autosomal recessive ataxias, CNS Neurol. Disord. Targets (Formerly Curr, Drug Targets-CNS Neurol. Disord. 17 (2018) 161–171.
[6] O. Audet, H.T. Bui, M. Allisse, A.-S. Comtois, M. Leone, Assessment of the impact of an exercise program on the physical and functional capacity in patients with autosomal recessive spastic ataxia of Charlevoix-Saguenay: An exploratory study, Intractable Rare Dis, Res. (2018).
[7] J.J.E. Mulvihill, E.M. Cunnane, A.M. Ross, J.T. Duskey, G. Tosi, A.M. Grabrucker, Drug delivery across the blood–brain barrier: recent advances in the use of nanocarriers, Nanomedicine. 15 (2020) 205–214.
[8] A. Puri, K. Loomis, B. Smith, J.-H. Lee, A. Yavlovich, E. Heldman, R. Blumenthal, Lipid-based nanoparticles as pharmaceutical drug carriers: from concepts to clinic, Crit. Rev. Ther. Drug Carr. Syst. 26 (2009).
[9] N.J. Abbott, Blood–brain barrier structure and function and the challenges for CNS drug delivery, J. Inherit. Metab. Dis. 36 (2013) 437–449.
[10] C. Tapeinos, M. Battaglini, G. Ciofani, Advances in the design of solid lipid nanoparticles and nanostructured lipid carriers for targeting brain diseases, J. Control. Release. 264 (2017) 306–332.
[11] N. Naseri, H. Valizadeh, P. Zakeri-Milani, Solid Lipid Nanoparticles and Nanostructured Lipid Carriers: Structure, Preparation and Application, Adv. Pharm. Bull. 5 (2015) 305–313, https://doi.org/10.15171/apb.2015.043.
[12] S. Dolatabadi, M. Karimi, S. Nasirizadeh, M. Hatamipour, S. Golmohammadzadeh, M.R. Jaafari, Preparation, characterization and in vivo pharmacokinetic evaluation of curcuminoids-loaded solid lipid nanoparticles (SLNs) and nanostructured lipid carriers (NLCs), J. Drug Deliv Sci. Technol. (2021) 102352.
[13] W.M. Lim, P.S. Rajinikanth, C. Mallikarjun, Y.B. Kang, Formulation and delivery of itraconazole to the brain using a nanolipid carrier system, Int. J. Nanomedicine. 9 (2014) 2117.
[14] C. Martinelli, M. Battaglini, C. Pucci, S. Gioi, C. Caracci, G. Macaluso, S. Doccini, F.M. Santorelli, G. Ciofani, Development of Nanostructured Lipid Carriers for the Delivery of Idebenone in Autosomal Recessive Spastic Ataxia of Charlevoix-Saguenay, ACS Omega. 5 (2020) 12451–12466.
[15] C. Tapeinos, A. Marino, M. Battaglini, S. Migliorin, R. Brescia, A. Scarpellini, C.D. J. Fernández, M. Prato, F. Drago, G. Ciofani, Stimuli-responsive lipid-based magnetic nanovectors increase apoptosis in glioblastoma cells through synergic intracellular hyperthermia and chemotherapy, Nanoscale. 11 (2019) 72–88.
[16] B. De Filippis, L. De Lellis, R. Florio, A. Ammazzalorso, P. Amoia, M. Fantacuzzi, L. Giampietro, C. Maccallini, R. Amoroso, S. Veschi, Synthesis and cytotoxic effects on pancreatic cancer cells of resveratrol analogs, Med. Chem. Res. 28 (2019) 984–991.
[17] R. Ahmadi, M.A. Ebrahimzadeh, Resveratrol–A comprehensive review of recent advances in anticancer drug design and development, Eur. J. Med. Chem. 112356 (2020).
[18] S.S. Leonard, C. Xia, B.-H. Jiang, B. Stinefelt, H. Klandorf, G.K. Harris, X. Shi, Resveratrol scavenges reactive oxygen species and effects radical-induced cellular responses, Biochem. Biophys. Res. Commun. 309 (2003) 1017–1026.
[19] S.S. Karuppagounder, J.T. Pinto, H. Xu, H.-L. Chen, M.F. Beal, G.E. Gibson, Dietary supplementation with resveratrol reduces plaque pathology in a transgenic model of Alzheimer's disease, Neurochem. Int. 54 (2009) 111–118.
[20] V. Vingtdeux, L. Giliberto, H. Zhao, P. Chandakkar, Q. Wu, J.E. Simon, E.M. Janle, J. Lobo, M.G. Ferruzzi, P. Davies, P. Marambaud, AMP-activated protein kinase signaling activation by resveratrol modulates amyloid-beta peptide metabolism, J. Biol. Chem. 285 (2010) 9100–9113, https://doi.org/10.1074/jbc.M109.060061.
[21] E.H. Gokce, E. Korkmaz, E. Dellera, G. Sandri, M.C. Bonferoni, O. Ozer, Resveratrol-loaded solid lipid nanoparticles versus nanostructured lipid carriers: evaluation of antioxidant potential for dermal applications, Int. J. Nanomedicine. 7 (2012) 1841–1850, https://doi.org/10.2147/IJN.S29710.
[22] J.A. Loureiro, S. Andrade, A. Duarte, A.R. Neves, J.F. Queiroz, C. Nunes, E. Sevin, L. Fenart, F. Gosselet, M.A.N. Coelho, Resveratrol and grape extract-loaded solid lipid nanoparticles for the treatment of Alzheimer's disease, Molecules. 22 (2017) 277.
[23] M. Elmowafy, H.M. Ibrahim, M.A. Ahmed, K. Shalaby, A. Salama, H. Hefesha, Atorvastatin-loaded nanostructured lipid carriers (NLCs): strategy to overcome oral delivery drawbacks, Drug Deliv. 24 (2017) 932–941.
[24] V. Sanna, A.M. Roggio, S. Siliani, M. Piccinini, S. Marceddu, A. Mariani, M. Sechi, Development of novel cationic chitosan-and anionic alginate–coated poly (d, l-lactide-co-glycolide) nanoparticles for controlled release and light protection of resveratrol, Int. J. Nanomedicine. 7 (2012) 5501.
[25] L. Qin, T. Lu, Y. Qin, Y. He, N. Cui, A. Du, J. Sun, In Vivo Effect of Resveratrol-Loaded Solid Lipid Nanoparticles to Relieve Physical Fatigue for Sports Nutrition Supplements, Molecules. 25 (2020) 5302.
[26] A. Alex, W. Paul, A.J. Chacko, C.P. Sharma, Enhanced delivery of lopinavir to the CNS using Compritol®-based solid lipid nanoparticles, Ther. Deliv. 2 (2011) 25–35.
[27] A.R. Neves, M. Lúcio, S. Martins, J.L.C. Lima, S. Reis, Novel resveratrol nanodelivery systems based on lipid nanoparticles to enhance its oral bioavailability, Int. J. Nanomedicine. 8 (2013) 177.
[28] B. Hernández, F. Pflüger, S.G. Kruglik, M. Ghomi, Characteristic Raman lines of phenylalanine analyzed by a multiconformational approach, J. Raman Spectrosc. 44 (2013) 827–833.
[29] T.Y. Bradshaw, L.E.L. Romano, E.J. Duncan, S. Nethisinghe, R. Abeti, G.J. Michael, P. Giunti, S. Vermeer, J.P. Chapple, A reduction in Drp1-mediated fission compromises mitochondrial health in autosomal recessive spastic ataxia of Charlevoix Saguenay, Hum. Mol. Genet. 25 (2016) 3232–3244.
[30] C. Criscuolo, C. Procaccini, M.C. Meschini, A. Cianflone, R. Carbone, S. Doccini, D. Devos, C. Nesti, I. Vuillaume, M. Pellegrino, Powerhouse failure and oxidative damage in autosomal recessive spastic ataxia of Charlevoix-Saguenay, J. Neurol. 262 (2015) 2755–2763.
[31] E.J. Duncan, R. Larivière, T.Y. Bradshaw, F. Longo, N. Sgarioto, M.J. Hayes, L.E.L. Romano, S. Nethisinghe, P. Giunti, M.B. Bruntraeger, Altered organization of the intermediate filament cytoskeleton and relocalization of proteostasis modulators in cells lacking the ataxia protein sacsin, Hum. Mol. Genet. 26 (2017) 3130–3143.
[32] B. Catalgol, S. Batirel, Y. Taga, N.K. Ozer, Resveratrol: French paradox revisited, Front. Pharmacol. 3 (2012) 141.
[33] J.-H. Kim, E.-Y. Park, H.-K. Ha, C.-M. Jo, W.-J. Lee, S.S. Lee, J.W. Kim, Resveratrol-loaded nanoparticles induce antioxidant activity against oxidative stress, Asian-Australasian J. Anim. Sci. 29 (2016) 288.
[34] E.M. Yiu, G. Tai, R.E. Peverill, K.J. Lee, K.D. Croft, T.A. Mori, B. Scheiber-Mojdehkar, B. Sturm, M. Praschberger, A.P. Vogel, An open-label trial in Friedreich ataxia suggests clinical benefit with high-dose resveratrol, without effect on frataxin levels, J. Neurol. 262 (2015) 1344–1353.
[35] M.H. Aburahma, S.M. Badr-Eldin, Compritol 888 ATO: a multifunctional lipid excipient in drug delivery systems and nanopharmaceuticals, Expert Opin. Drug Deliv. 11 (2014) 1865–1883.
[36] A.A.M. Shimojo, A.R.V. Fernandes, N.R.E. Ferreira, E. Sanchez-Lopez, M.H.A. Santana, E.B. Souto, Evaluation of the Influence of Process Parameters on the Properties of Resveratrol-Loaded NLC Using 2(2) Full Factorial Design, Antioxidants (Basel, Switzerland). 8 (2019) 272, https://doi.org/10.3390/antiox8080272.
[37] W.H. De Jong, P.J.A. Borm, Drug delivery and nanoparticles: applications and hazards, Int. J. Nanomedicine. 3 (2008) 133.
[38] M. Haider, S.M. Abdin, L. Kamal, G. Orive, Nanostructured lipid carriers for delivery of chemotherapeutics: A review, Pharmaceutics. 12 (2020) 288.

[39] R.A. Kore, E.C. Abraham, Inflammatory cytokines, interleukin-1 beta and tumor necrosis factor-alpha, upregulated in glioblastoma multiforme, raise the levels of CRYAB in exosomes secreted by U373 glioma cells, Biochem. Biophys. Res. Commun. 453 (2014) 326–331.
[40] W. Chen, X.I.A. Zhang, W. Huang, Role of neuroinflammation in neurodegenerative diseases, Mol. Med. Rep. 13 (2016) 3391–3396.
[41] M. Erta, A. Quintana, J. Hidalgo, Interleukin-6, a major cytokine in the central nervous system, Int. J. Biol. Sci. 8 (2012) 1254.
[42] T. Tanaka, M. Narazaki, T. Kishimoto, IL-6 in inflammation, immunity, and disease, Cold Spring Harb. Perspect. Biol. 6 (2014) a016295.
[43] D.D. Lofrumento, G. Nicolardi, A. Cianciulli, F. De Nuccio, V. La Pesa, V. Carofiglio, T. Dragone, R. Calvello, M.A. Panaro, Neuroprotective effects of resveratrol in an MPTP mouse model of Parkinson's-like disease: possible role of SOCS-1 in reducing pro-inflammatory responses, Innate Immun. 20 (2014) 249–260.
[44] Y.-C. Oh, O.-H. Kang, J.-G. Choi, H.-S. Chae, Y.-S. Lee, O.-O. Brice, H.J. Jung, S.-H. Hong, Y.-M. Lee, D.-Y. Kwon, Anti-inflammatory effect of resveratrol by inhibition of IL-8 production in LPS-induced THP-1 cells, Am. J. Chin. Med. 37 (2009) 1203–1214.
[45] R. Kolahdouz-Mohammadi, F. Shidfar, S. Khodaverdi, T. Arablou, S. Heidari, N. Rashidi, A. Delbandi, Resveratrol treatment reduces expression of MCP-1, IL-6, IL-8 and RANTES in endometriotic stromal cells, J. Cell. Mol. Med. 25 (2021) 1116–1127.
[46] T.R. Burton, S.B. Gibson, The role of Bcl-2 family member BNIP3 in cell death and disease: NIPping at the heels of cell death, Cell Death Differ. 16 (2009) 515–523.
[47] D. Baetz, K. Ens, J. Shaw, S. Kothari, N. Yurkova, L.A. Kirshenbaum, Nuclear factor-kappaB-mediated cell survival involves transcriptional silencing of the mitochondrial death gene BNIP3 in ventricular myocytes, PG - 3777–85 (2005), https://doi.org/10.1161/CIRCULATIONAHA.105.573899.
[48] S. Pan, S.D. Shah, R.A. Panettieri Jr, D.A. Deshpande, Bnip3 regulates airway smooth muscle cell focal adhesion and proliferation, Am. J. Physiol. Cell. Mol. Physiol. 317 (2019) L758–L767.
[49] M.A. Iddah, B.N. Macharia, Autoimmune thyroid disorders, ISRN Endocrinol. 2013 (2013), https://doi.org/10.1155/2013/509764 509764.
[50] E. Afreen, M. Humayun, A. Sheikh, Neurological spectrum of diseases associated with autoimmune thyroid disease: a case series to recognize diagnostically helpful signs.(P1. 347), 2018.
[51] I. Correia, I.B. Marques, R. Ferreira, L. Sousa, Encephalopathy Associated with Autoimmune Thyroid Disease: A Potentially Reversible Condition, Case Rep. Med. 2016 (2016) 9183979, https://doi.org/10.1155/2016/9183979.
[52] P. Habibzadeh, Z. Tabatabaei, S. Inaloo, M.M. Nashatizadeh, M. Synofzik, V.R. Ostovan, M.A. Faghihi, Case Report: Expanding the Genetic and Phenotypic Spectrum of Autosomal Recessive Spastic Ataxia of Charlevoix-Saguenay, Front. Genet. 11 (2020).
[53] C. Giuliani, M. Iezzi, L. Ciolli, A. Hysi, I. Bucci, S. Di Santo, C. Rossi, M. Zucchelli, G. Napolitano, Resveratrol has anti-thyroid effects both in vitro and in vivo, Food Chem. Toxicol. 107 (2017) 237–247.
[54] I. Miljkovic, L.M. Yerges, H. Li, C.L. Gordon, B.H. Goodpaster, L.H. Kuller, C.S. Nestlerode, C.H. Bunker, A.L. Patrick, V.W. Wheeler, Association of the CPT1B gene with skeletal muscle fat infiltration in Afro-Caribbean men, Obesity. 17 (2009) 1396–1401.
[55] L. Zhang, H. Li, X. Hu, D.M. Benedek, C.S. Fullerton, R.D. Forsten, J.A. Naifeh, X. Li, H. Wu, K.N. Benevides, T. Le, S. Smerin, D.W. Russell, R.J. Ursano, Mitochondria-focused gene expression profile reveals common pathways and CPT1B dysregulation in both rodent stress model and human subjects with PTSD, Transl. Psychiatry. 5 (2015) e580, https://doi.org/10.1038/tp.2015.65.
[56] Y. Zhang, X. Fang, M. Dai, Q. Cao, T. Tan, W. He, Y. Huang, L. Chu, M. Bao, Cardiac-specific down-regulation of carnitine palmitoyltransferase-1b (CPT-1b) prevents cardiac remodeling in obese mice, Obesity. 24 (2016) 2533–2543.
[57] M. Savarese, J. Sarparanta, A. Vihola, B. Udd, P. Hackman, Increasing Role of Titin Mutations in Neuromuscular Disorders, J. Neuromuscul. Dis. 3 (2016) 293–308, https://doi.org/10.3233/JND-160158.
[58] S.J. Beecroft, K.S. Yau, R.J.N. Allcock, K. Mina, R. Gooding, F. Faiz, V.J. Atkinson, C. Wise, P. Sivadorai, D. Trajanoski, Targeted gene panel use in 2249 neuromuscular patients: the Australasian referral center experience, Ann. Clin. Transl. Neurol. 7 (2020) 353–362.
[59] Q. Lu, L. Shang, W.T. Tian, L. Cao, X. Zhang, Q. Liu, Complicated paroxysmal kinesigenic dyskinesia associated with SACS mutations, Ann. Transl. Med. 8 (2020).
[60] M. Savarese, L. Maggi, A. Vihola, P.H. Jonson, G. Tasca, L. Ruggiero, L. Bello, F. Magri, T. Giugliano, A. Torella, Interpreting genetic variants in titin in patients with muscle disorders, JAMA Neurol. 75 (2018) 557–565.
[61] T. Geuens, D. Bouhy, V. Timmerman, The hnRNP family: insights into their role in health and disease, Hum. Genet. 135 (2016) 851–867, https://doi.org/10.1007/s00439-016-1683-5.
[62] S. Cho, H. Moon, T.J. Loh, H.K. Oh, S. Cho, H.E. Choy, W.K. Song, J.-S. Chun, X. Zheng, H. Shen, hnRNP M facilitates exon 7 inclusion of SMN2 pre-mRNA in spinal muscular atrophy by targeting an enhancer on exon 7, Biochim. Biophys. Acta (BBA)-Gene Regul. Mech. 1839 (2014) 306–315.
[63] Q. Liu, S. Shu, R.R. Wang, F. Liu, B. Cui, X.N. Guo, C.X. Lu, X.G. Li, M.S. Liu, B. Peng, Whole-exome sequencing identifies a missense mutation in hnRNPA1 in a family with flail arm ALS, Neurology. 87 (2016) 1763–1769.
[64] S. Lee, M. Levin, Novel somatic single nucleotide variants within the RNA binding protein hnRNP A1 in multiple sclerosis patients F1000Research (2014) 3.
[65] K.M. Pollard, P. Hultman, Fibrillarin autoantibodies, in: Autoantibodies, Elsevier, 2014, pp. 319–325.
[66] D.G. Dimitrova, L. Teysset, C. Carré, RNA 2′-O-methylation (Nm) modification in human diseases, Genes (Basel). 10 (2019) 117.
[67] S.Y. Moon, Y. Zheng, Rho GTPase-activating proteins in cell regulation, Trends Cell Biol. 13 (2003) 13–22.
[68] L. Castellani, E. Salvati, S. Alema, G. Falcone, Fine regulation of RhoA and Rock is required for skeletal muscle differentiation, J. Biol. Chem. 281 (2006) 15249–15257.
[69] K. Iwasaki, K. Hayashi, T. Fujioka, K. Sobue, Rho/Rho-associated kinase signal regulates myogenic differentiation via myocardin-related transcription factor-A/Smad-dependent transcription of the Id3 gene, J. Biol. Chem. 283 (2008) 21230–21241, https://doi.org/10.1074/jbc.M710525200.
[70] J.T. Doherty, K.C. Lenhart, M.V. Cameron, C.P. Mack, F.L. Conlon, J.M. Taylor, Skeletal muscle differentiation and fusion are regulated by the BAR-containing Rho-GTPase-activating protein (Rho-GAP), GRAF1, J. Biol. Chem. 286 (2011) 25903–25921, https://doi.org/10.1074/jbc.M111.243030.
[71] B.L. Fogel, S. Perlman, Clinical features and molecular genetics of autosomal recessive cerebellar ataxias, Lancet Neurol. 6 (2007) 245–257.
[72] A.H. Crosby, H. Patel, B.A. Chioza, C. Proukakis, K. Gurtz, M.A. Patton, R. Sharifi, G. Harlalka, M.A. Simpson, K. Dick, Defective mitochondrial mRNA maturation is associated with spastic ataxia, Am. J. Hum. Genet. 87 (2010) 655–660.
[73] M. Beaudin, A. Matilla-Dueñas, B.-W. Soong, J.L. Pedroso, O.G. Barsottini, H. Mitoma, S. Tsuji, J.D. Schmahmann, M. Manto, G.A. Rouleau, C. Klein, N. Dupre, The Classification of Autosomal Recessive Cerebellar Ataxias: a Consensus Statement from the Society for Research on the Cerebellum and Ataxias Task Force, Cerebellum. 18 (2019) 1098–1125, https://doi.org/10.1007/s12311-019-01052-2.
[74] F. Morani, S. Doccini, G. Chiorino, F. Fattori, D. Galatolo, E. Sciarrillo, F. Gemignani, S. Zuchner, E. Bertini, F.M. Santorelli, Functional Network Profiles in ARSACS Disclosed by Aptamer-Based Proteomic Technology, Front. Neurol. 11 (2020) 1883.
[75] M. Agrawal, S. Saraf, S. Saraf, S.K. Dubey, A. Puri, R.J. Patel, V. Ravichandiran, U. S. Murty, A. Alexander, Recent strategies and advances in the fabrication of nano lipid carriers and their application towards brain targeting, J. Control. Release. 321 (2020) 372–415.
[76] N.A. Kulak, G. Pichler, I. Paron, N. Nagaraj, M. Mann, Minimal, encapsulated proteomic-sample processing applied to copy-number estimation in eukaryotic cells, Nat. Methods. 11 (2014) 319.
[77] Y. Perez-Riverol, A. Csordas, J. Bai, M. Bernal-Llinares, S. Hewapathirana, D.J. Kundu, A. Inuganti, J. Griss, G. Mayer, M. Eisenacher, The PRIDE database and related tools and resources in 2019: improving support for quantification data, Nucleic Acids Res. 47 (2019) D442–D450.
[78] J. Cox, M. Mann, MaxQuant enables high peptide identification rates, individualized ppb-range mass accuracies and proteome-wide protein quantification, Nat. Biotechnol. 26 (2008) 1367–1372.
[79] S. Tyanova, T. Temu, P. Sinitcyn, A. Carlson, M.Y. Hein, T. Geiger, M. Mann, J. Cox, The Perseus computational platform for comprehensive analysis of (prote) omics data, Nat. Methods. 13 (2016) 731.